# High-repetition rate ultrafast burst laser processing of copper and silicon up to 15 GHz.

Valeria Viviana Belloni, Maxime Pinaud, Hugo Delahaye, Luca Furfaro, Lilia Pontagnier, Giorgio Santarelli, Eric Cormier, Luc Froehly, François Courvoisier

# High-repetition rate ultrafast burst laser processing of copper and silicon up to 15 GHz

Valeria V. Belloni,[1,*] Maxime Pinaud,[1] Hugo Delahaye,[1] Luca Furfaro, [1] Lilia Pontagnier,[2], Giorgio Santarelli,[2] Eric Cormier,[2] Luc Froehly, [1] and Francois Courvoisier [1,**]
[1] Université Marie et Louis Pasteur, CNRS, institut FEMTO-ST, F-25000 Besançon, France
[2] Laboratoire Photonique Numérique et Nanosciences (LP2N), UMR 5298, CNRS-IOGS-Université Bordeaux, 33400 Talence, France
[*] valeria.belloni@femto-st.fr
[**] francois.courvoisier@femto-st.fr

This article has been published in open access in *Optical Express*.
Its full reference is:
Valeria V. Belloni, Maxime Pinaud, Hugo Delahaye, Luca Furfaro, Lilia Pontagnier, Giorgio Santarelli, Eric Cormier, Luc Froehly, and Francois Courvoisier, "High-repetition rate ultrafast burst laser processing of copper and silicon up to 15 GHz," Optics Express 33, 26139-26151 (2025)
https://doi.org/10.1364/OE.558402

**Ultrafast lasers are widely used in microfabrication due to their precision and minimal thermal damage, but their throughput is often limited. Processing with bursts of pulses with GHz repetition rates aims to enhance ablation efficiency. However, recent results have shown strong dependencies on the number of pulses within the burst. The present work focuses on the pulse repetition rate. We report ultrafast laser ablation in copper and silicon at unexplored intra-burst repetition rates, from 1 up to 15 GHz, in both single and multi-burst processing. High resolution scanning electron microscopy is used to characterize ablation volumes and crater morphology. Our results demonstrate a benefit in the ablation efficiency at very high repetition rates in the case of copper. It also shows that optimal processing for silicon and copper is observed with very different parameter configurations. This difference is attributed to the different thermal diffusivities. In addition, the crater morphologies across the different studied configurations strongly suggest a dependency on the viscosity of the liquid phase, providing insight into the varying temperatures reached during ablation.**

## 1 Introduction

Ultrafast lasers have become indispensable in microfabrication due to their precision and ability to minimize thermal damage [1]. By confining the energy deposition process into an extremely short time scale, ultrafast lasers can achieve clean ablation with minimal heat diffusion, making them ideal for applications that require precise patterning. However, the throughput of machining with ultrafast laser is usually lower than longer pulses [2]. While ultrashort pulses reduce heat diffusion, the thermal load remains a major challenge: as a significant fraction of the absorbed energy does not leave the material with ablation, increasing further pulse energy causes unwanted melting, cracking, or thermal stress.

In 2016, Kerse *et al.* showed that bursts of pulses with GHz repetition rate allow for a much cleaner and precise ablation [3]. At GHz repetition frequencies, laser ablation enters an interaction regime where cumulative heating becomes significant. Due to the short delay between pulses, heat accumulation in a nm- thin surface layer leads to rapid temperature build-up and causes the material to reach the ablation threshold. As mechanism explanation, Kerse *et al.* proposed the 'ablation-cooled' model in which, after reaching the ablation threshold, each sub-pulse in the burst ablates a small layer of material, effectively removing the heat energy with it [3]. Further research on laser processing in the GHz burst regime reveals mixed findings on its effectiveness [4, 5, 6, 7]. In fact, it is the differences in burst characteristics, processing techniques, and material types that highly influence the conclusions. For meaningful comparisons, it is therefore crucial to compare the evolution with respect to the number of pulses and the GHz intra-burst repetition rate.

Here, thanks to a new concept of laser oscillator [8], we investigate GHz burst ablation in a highly flexible set of parameters. We vary intra-burst pulse number from 50 to 1500 and in a previously inaccessible regime of very high repetition rate. While previous literature reported measurements up to 5.4 GHz [9], we investigate laser ablation with intra-burst repetition rate up to $15\,\mathrm{GHz}$. This large range in repetition rate is important because it crosses the threshold at $4\,\mathrm{GHz}$ for heat accumulation in copper as will be detailed below.

We have investigated 15 different burst configurations in single burst and percussion drilling regimes for silicon and copper. To obtain high accuracy in our results, we performed SEM measurements to calculate the ablated volume and the *ablation efficiency*, defined as the ablated volume divided by the total burst energy. We show that the morphology of the craters and the surrounding ejecta can be explained by the viscosity of the liquid phase and provide insight into the different temperatures reached by the material. We observe that a higher repetition rate improves ablation efficiency on copper, while for silicon, repetition rates above $1\,\mathrm{GHz}$ have a minor impact on the ablation efficiency. The different thermal diffusivities of the materials explain the different responses to the repetition rates. Finally, percussion drilling shows an evolution of the crater shape with the burst duration, which is consistent with a less efficient material expulsion.

## 2 Experimental procedure

**Laser system and processing setup** The laser system is a prototype developed in the kW-flexiburst project operating at $1030\,\mathrm{nm}$. The pulse duration is $1.5 \pm 0.3$ ps and the bursts show a uniform energy distribution among the sub-pulses. The laser burst can be arbitrarily programmed to change the intra-burst repetition rate (from $1\,\mathrm{GHz}$ to $18\,\mathrm{GHz}$), the inter-burst repetition rate (from $0.1\,\mathrm{MHz}$ to $20\,\mathrm{MHz}$), and the number of pulses per burst (ppb, from 10 to 1000s). In this study, we concentrated our efforts on the effect of the intra-burst repetition rate and the number of pulses. We selected combinations of those two parameters to produce bursts of durations between $33\,\mathrm{ns}$ and $200\,\mathrm{ns}$ as burst duration was shown to be critical for silicon ablation [5]. Table 1 reports all the tested configurations. For the sake of simplicity, we will refer to the intra-burst repetition rate as the "repetition rate". We note that for repetition rates of 5 and 11 GHz, technical limitations of the laser prototype imposed that fewer configurations were

| Intra-burst rep. rate | 1 GHz | | | 1.5 GHz | | | 3 GHz | | | 5 GHz | 11 GHz | | 15 GHz | | |
|---|---|---|---|---|---|---|---|---|---|---|---|---|---|---|---|
| Pulses per burst | 50 | 100 | 200 | 50 | 100 | 150 | 100 | 200 | 300 | 100 | 220 | 1100 | 500 | 1000 | 1500 |
| Burst duration (ns) | 50 | 100 | 200 | 33 | 66 | 100 | 33 | 66 | 100 | 20 | 20 | 100 | 33 | 66 | 100 |

Table 1: Configurations used for processing the samples.

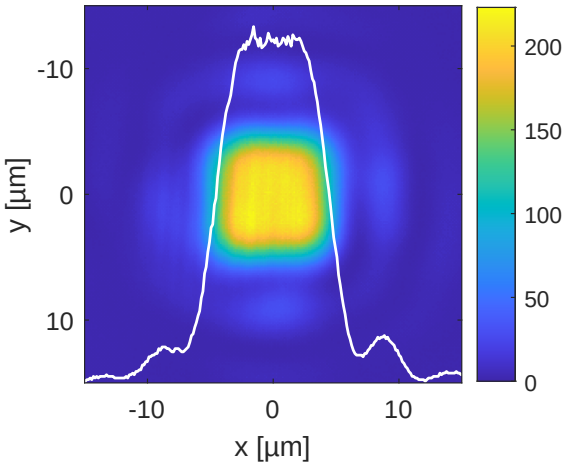


Figure 1: Cross-cut and intensity profile (white curve) of the beam at the sample position.

possible.

The Gaussian beam is shaped in a squared flat top with the CANUNDA-PULSE module (Cailabs). The beam is then demagnified with a 4f system ($f = 500\,\mathrm{mm}$ lens and microscope objective NA=0.4). On the sample surface, the beam has dimensions (FWHM) of $9.2\,\mu\mathrm{m} \times 9.6\,\mu\mathrm{m}$ as shown in Fig. 1. The experiments have been performed in ambient air. We first performed experiments on silicon and copper in single burst to study crater morphology (section 3) and single burst ablation efficiency (section 4). Then, to study the efficiency and morphology in the regime of percussion drilling (section 5), we superimposed 10 bursts at 10 kHz inter-burst repetition rate without changing the relative beam-sample position. The sample was mounted on a 3-axis translation stage and two rotation stages to ensure the sample is perpendicular to the beam and at the focal point. We performed a series of ten to twelve ablations for each selected configuration at different powers.

**Crater imaging** For high-resolution imaging of the craters, we used Scanning Electron Microscope (SEM) imaging and a Focused Ion Beam (FIB) milling. We milled with the FIB half of the crater to provide access to a cross-section view. We measured the dimensions of the ablated craters to retrieve the ablated volume. From the ablated volumes, we obtained ablation efficiency as a function of the burst fluence for each configuration. We calculated the ablation efficiency as the ablated volume in $\mathrm{mm}^3$

divided by the laser power in W and $\Delta t$ in minutes. In the case of single-burst processing, $\Delta t$ represents the time between two consecutive bursts. For the 10-burst processing, this value is multiplied by a factor of 10. From the curves, we retrieved the optimal ablation efficiency and the optimal fluence, which are the coordinates of the maximum of the curve. We also extrapolated the fluence threshold for the single-burst processing, which represents the minimum fluence required to induce modifications in the samples.

## 3 Single burst crater morphology

Before investigating in detail the ablation threshold and efficiency for the different configurations, we report on the morphologies observed. Fig. 2 shows the SEM images of laser impacts performed with a single burst at $1.5\,\mathrm{GHz}$ with 150 pulses in the case of silicon and $15\,\mathrm{GHz}$ with 1500 pulses in the case of copper. The evolution of the morphologies obtained with the other laser configurations are qualitatively very similar to those presented here for each material.

In each row, the fluence increases from left, just above fluence threshold ($\approx 11\,\mathrm{J\,cm^{-2}}$ for both materials), to the right at the optimal ablation efficiency. In the case of silicon, a burst with fluence just above threshold leads to the formation of a pool of resolidified liquid material with a central bump, as already observed by Mishchik *et al*[10]. By increasing the fluence, we can observe how the molten material starts to be pushed outwards until the creation of a proper crater, where the liquid material is expelled outside the cavity. In the case of copper just above threshold, the material is molten and resolidified without a particular shape. At higher fluence, the molten material is pushed towards the side of the cavity creating a rim of material with uneven thickness. At the optimal fluence, the rim is a vertical thin wall of copper with a thickness of typically 60 to $80\,\mathrm{nm}$ and a couple of micrometers high. A similar rim has been observed on copper in a previous experiment in the GHz regime [11].

Despite the 'ablation cooling' model presenting the ablation as the evaporation of a thin layer of material per sub-pulse [3], our experiments show that the crater is formed also with the ejection of a significant amount of molten material even at the fluence of maximal ablation efficiency (see last craters in Fig. 2). A recent study showed, through time-resolved scattering imaging, that GHz bursts have two main mechanisms of material removal: the first is the vaporization of part of material followed by, secondly, the expulsion of molten material at high speed due to a radially outward liquid motion caused by the generated recoil pressure. The material with insufficient momentum resolidifies into a rim [11]. Our experiments are in agreement with this mechanism and show a significant amount of nano-particles in a radius of about $100\,\mu\mathrm{m}$ around the craters for silicon and $50\,\mu\mathrm{m}$ for copper, associated with micro-droplets at the edge of the craters for silicon and the thin rim for copper.

The generation of similar high rims around laser-induced craters has been already observed on thin film of silver [13]. The rim produced by a laser pulse is comparable to the one produced by a drop impinging onto a liquid layer. The shape of the splash strongly changes depending on the liquid physical properties, the reservoir thickness or the droplet speed. Fig. 3, adapted from Ref. [12], compares, in

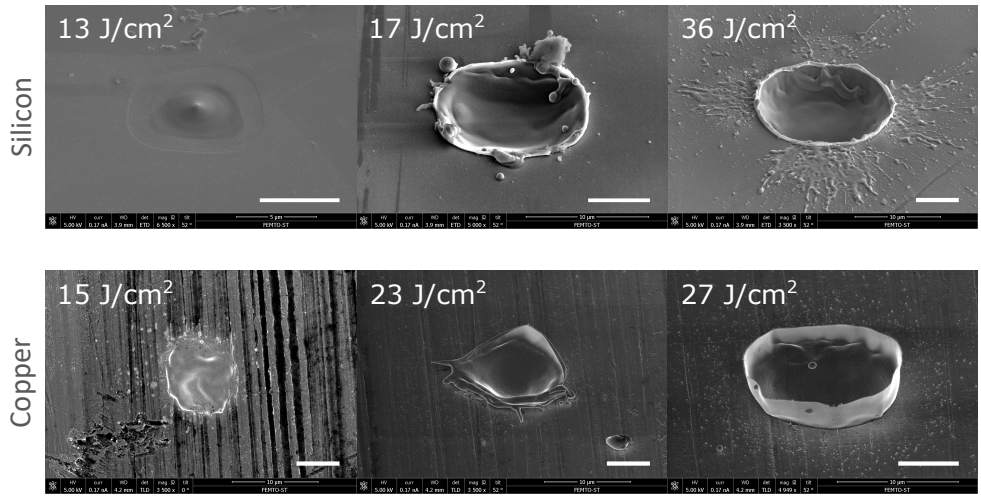


Figure 2: Morphology of the ablation for silicon (1.5 GHz burst with 150 pulses) and copper (15 GHz burst with 1500 pulses) for different fluences. The craters on the right are at the optimal fluence. Scale bars are 5 µm.

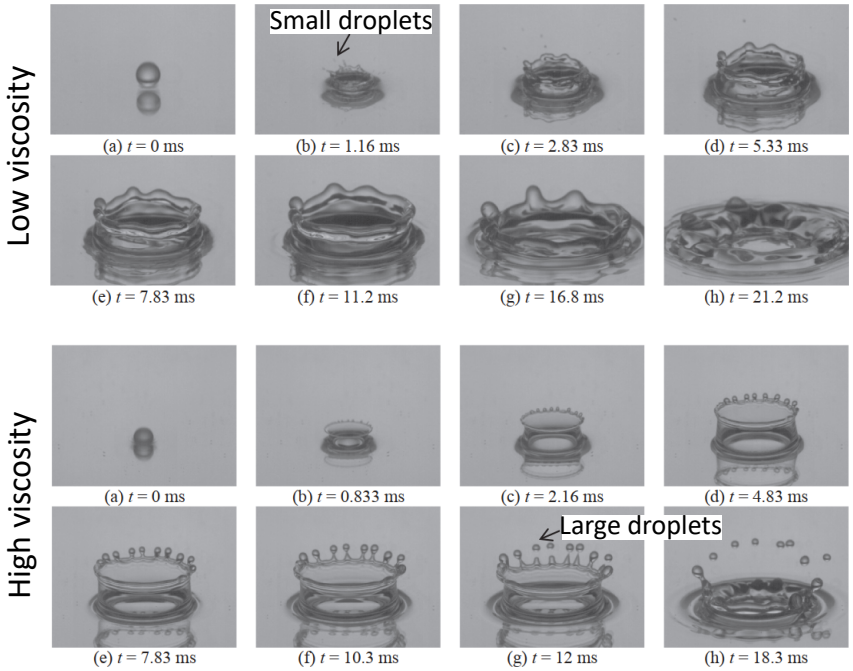


Figure 3: Images of the rims generated after the impact of a droplet on a still liquid at different times. In the case of low viscosity, the liquid is water. In the case of high viscosity, the liquid is a 55% glycerol solution. Reprinted and adapted from Ref.[12], with permission from Elsevier.

such experiment, the temporal dynamics of the splash for two different values of viscosity, using water (low viscosity) and glycerol solution (high viscosity). In the case of low viscosity of the liquid layer (top rows), the rim quickly tends to break into small droplets, while for a more viscous liquid (bottom rows), a very thin and high rim of liquid is formed, which tends, at a later stage, to generate large droplets due to capillary instabilities. The coexistence of droplets produced at the beginning of the rim formation and due to its crowning is possible for intermediate viscosities [14].

Despite the complexity of the process and the number of parameters involved, we infer that the different rim morphologies observed for silicon and copper are related to the viscosity of their respective liquid phases. The viscosity of liquid copper ($\mu = 4\,\mathrm{mPa\,s}$ [15]) is almost seven times higher compared to the one of silicon ($\mu = 0.6\,\mathrm{mPa\,s}$ [16]). This is almost the same as the ratio between water ($\mu = 0.89\,\mathrm{mPa\,s}$) and glycerol solution of Fig.3 ($\mu = 5.04\,\mathrm{mPa\,s}$) [12].

In Fig. 2, the crater produced in silicon ablation at the optimal fluence is compatible with the low-viscosity scenario, associated to ejection of small droplets all around the crater. In contrast, in the case of copper, the very high and thin rim, associated to the absence of droplets around the crater, fits with the high-viscosity scenario. In this case, we infer that the freezing of the thin liquid rim takes place before the capillary instabilities could grow. We will see later that burst configurations for silicon induce morphologies sometimes in-between these scenarios.

## 4 Ablation efficiency in single burst regime

We started the evaluation of ablation threshold and efficiency (crater volume divided by total burst energy) in the regime of single burst processing. The ablation efficiency is a critical parameter for applications because it affects the processing performance. The concept of optimal ablation, initially developed for drilling with repeated single pulses [17], establishes a link between maximum ablation efficiency and optimal morphological outcomes. Therefore, to meaningfully compare the different configurations, we investigated the optimal fluence at which the ablation efficiency is the highest.

Figure 4 shows the ablation efficiency as a function of the total burst fluence for a representative selection of the studied configurations, both for silicon (left column) and copper (right column). The error bars on the ablation efficiency are given by the uncertainties in the calculation of the crater volume. The curves show that the range of fluence that we investigated is well calibrated to retrieve the fluence threshold and the optimal fluence at which the efficiency peaks. We qualitatively observe from Fig. 4 that the fluence threshold tends to increase with the burst duration, as well as the optimal fluence. For quantitative comparisons, we reported, for each of the 15 laser configurations, the values of fluence threshold, optimal fluence and optimal ablation efficiency as a function of the burst duration in Fig. 5.

**Fluence threshold and craters formation** We begin our analysis with the fluence threshold. As illustrated in Fig. 5, the fluence threshold rises with increasing burst duration for both materials. A higher number of pulses per burst results in lower-energy sub-pulses, causing the rise of the ablation threshold.

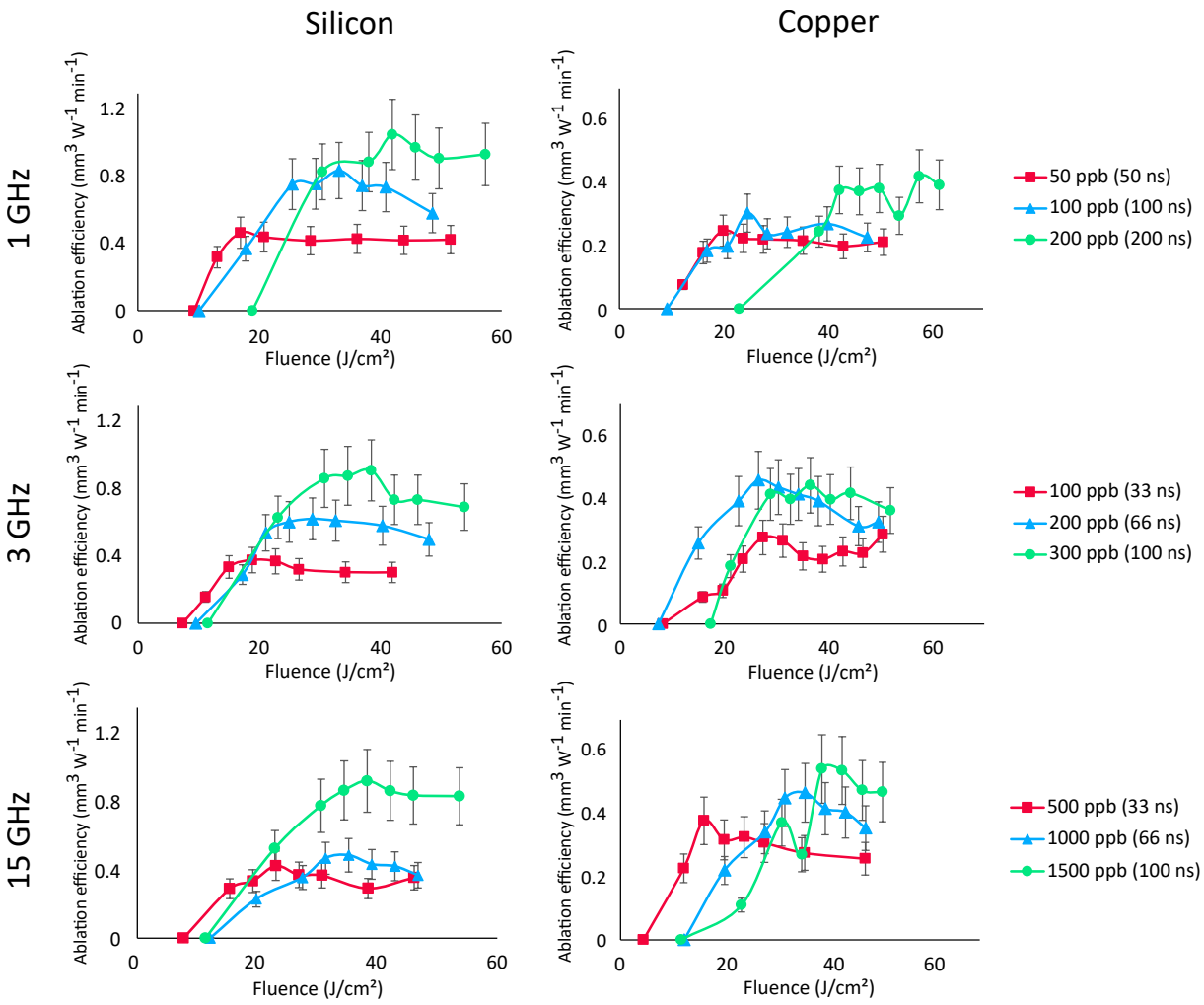


Figure 4: Ablation efficiency curves for different configurations at intra-burst repetition rates of 1 GHz, 3 GHz, and 15 GHz for silicon and copper.

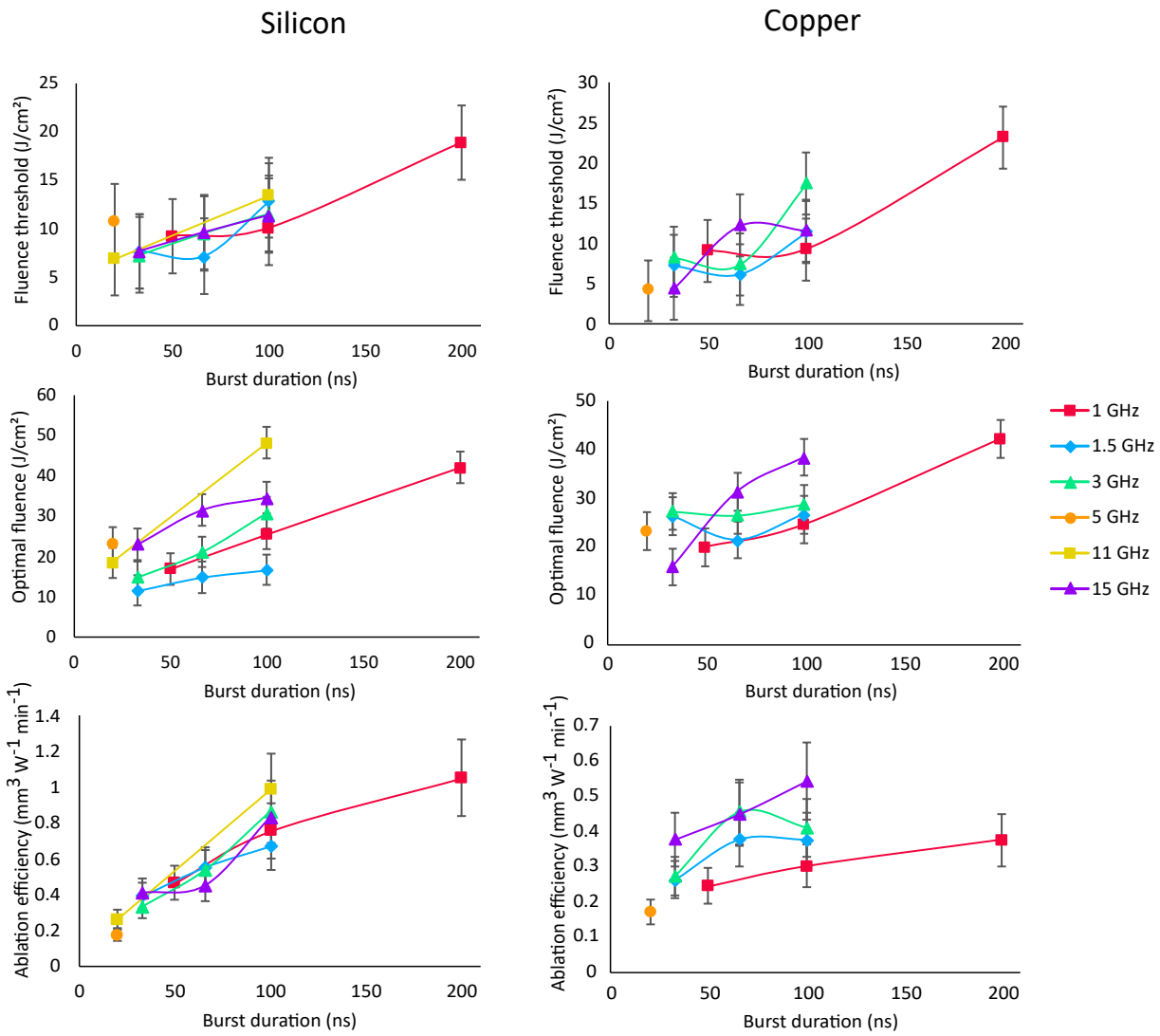


Figure 5: Fluence threshold, optimal fluence and ablation efficiency as a function of the burst duration for silicon and copper for the 15 different laser burst configurations.

We also notice that, for a given burst duration, the amplitude of the variation of the threshold fluence values across the different repetition rates is within the error bar of our measurement. Furthermore, the fluence threshold is similar for both materials, as what is observed in single-pulse ablation [18, 19]. It varies between $\approx 5\,\mathrm{J\,cm^{-2}}$ ($\approx 4\,\mu\mathrm{J}$ per burst) for short burst duration, up to $\approx 20\,\mathrm{J\,cm^{-2}}$ ($\approx 18\,\mu\mathrm{J}$ per burst) for the longest burst duration.

**Evolution of the optimal ablation fluence with burst configuration** Following Fig. 5, both materials show an increase of the optimal fluence for longer burst duration and a tendency of the optimal fluence to grow with the repetition rate (large number and less energetic sub-pulses). Silicon has its two-photon absorption coefficient peak approximately at the laser wavelength ($\approx 1\,\mu\mathrm{m}$) [20], therefore a burst with more sub-pulses needs a higher fluence to reach the optimal ablation. The absorption of copper increases rapidly with the temperature increase [21]. Therefore, the longer burst configurations with a higher number of pulses and lower fluence are less efficient to heat up the material and require a higher overall fluence to reach the optimal point.

The optimal ablation efficiencies of the different burst configurations are presented in Fig. 5 (bottom panel). For both materials, the ablation efficiency increases with the burst duration, as expected from the 'ablation cooling' mechanism [3]. While for silicon, the efficiency is quasi-independent of the intra-burst repetition rate, we see a nearly two-fold increase for copper between 1 and $15\,\mathrm{GHz}$. This behavior can be understood from the threshold repetition rate to reach heat accumulation. Silicon exhibits a thermal diffusivity $\alpha$ of $80\,\mathrm{mm\,s^{-2}}$ at $300\,\mathrm{K}$ and $8\,\mathrm{mm\,s^{-2}}$ at $1687\,\mathrm{K}$ (melting point) [22]. For a laser-excited layer $\delta$ of $100\,\mathrm{nm}$, the characteristic time for heat to dissipate from this layer can be estimated by $\tau_D \approx \frac{\delta^2}{\alpha}$ resulting in $0.12\,\mathrm{ns}$ at $300\,\mathrm{K}$ and $1.2\,\mathrm{ns}$ at $1687\,\mathrm{K}$ for silicon. Consequently, the repetition rate required to achieve heat accumulation is around $8\,\mathrm{GHz}$ at room temperature, decreasing to $0.8\,\mathrm{GHz}$ as the material reaches the melting point. For copper, using the same parameters, the required repetition rate is approximately $11.1\,\mathrm{GHz}$ at room temperature and 4 GHz at $1360\,\mathrm{K}$ (melting point) [23].

Since all the repetition rates we used are at least $1\,\mathrm{GHz}$, it is possible that an increase in the repetition rate does not bring an overall benefit to the ablation efficiency of silicon. Our results are in agreement with previous literature for silicon ablation for intra-burst repetition rates up to $3.5\,\mathrm{GHz}$ [5]. In agreement with this study, the longest burst leads to the highest ablation efficiency of $1\,\mathrm{mm^3/W/min}$ (200 pulses per burst at $1\,\mathrm{GHz}$), which is in the range presented in the literature with Gaussian beam [3, 5, 10, 24, 25]. We note that the absolute value of efficiency highly depends on spot size and on the exact definition of fluence.

In the case of copper, our data shows the increase of the optimal ablation efficiency with intra-burst repetition rate. This is because the range of investigated repetition rates crosses the $\sim 4\,\mathrm{GHz}$ threshold for heat accumulation. We measured the highest ablation efficiency of $0.5\,\mathrm{mm^3/W/min}$ with the burst at $15\,\mathrm{GHz}$ and 1500 pulses, which gives an $80\%$ increase compared to the burst of the same duration at $1\,\mathrm{GHz}$ with 100 pulses. This value is in line with previous literature (maximum repetition rate used $3.5\,\mathrm{GHz}$) [3, 5, 24, 25, 26].

As an example of quantitative agreement with literature, we compare our results in single burst to reference [24]. Our regime of 1 GHz, 200 ns burst duration (200 pulses) is comparable to 1.6 GHz, 250 ns burst duration (400 pulses). For this regime, we measured an ablation efficiency for silicon of 1 $mm^3$/min/W while it is 1.5 $mm^3$/min/W in ref. [24]. For copper, we measured 0.38 $mm^3$/min/W while it was at 0.39 in ref. [24].

**Comparison of crater morphologies at the optimal fluence** The quality of the ablation is an additional parameter that is important for most applications. Here, we compare the morphology of the craters in the different configurations. For meaningful comparisons, we chose, for each configuration, the fluence at which the ablation efficiency is maximal. The SEM images of the craters drilled in single burst are represented in Fig. 6 for silicon and in Fig. 7 for copper. The SEM images are sorted by increasing repetition rate from top to bottom and burst duration from left to right.

We start our comparison with the silicon sample (Fig. 6). The same burst duration (same column) leads to similar ablation efficiencies, it also leads to similar morphology. For short burst durations, the crater is square and is surrounded by relatively large droplets of molten materials with a typical diameter of 1-2 $\mu$m. When the burst duration is increased (towards the right side), the craters become circular and the large droplets around the craters are replaced by much smaller ones. We infer that heat diffusion plays a significant role in the ablation process.

The evolution of the droplet morphology can be interpreted with the generation of droplets by the laser pulses, as previously introduced. The larger droplets indicate a more viscous material, while the smaller droplets a less viscous material. Therefore, we infer that longer bursts allow the liquid material to reach higher temperatures in the thermal accumulation regime [3, 26]. While, for silicon, there is in general only a minor change in morphology with the repetition rate, we remark that, in the case of burst duration $100\,\mathrm{ns}$, craters from low repetition rates present only small droplets (low viscosity) while higher repetition rates (from $11\,\mathrm{GHz}$) still present large droplets. In the last case, the very low fluence of the single sub-pulses of the long burst duration at the highest repetition rates seems counterproductive because material ejection is less effective, probably because of the reduced two-photon absorption process leading to a smaller increase in the temperature of the molten pool. Finally, the cleanest ablation coincides with the highest ablation efficiency on silicon, with 200 pulses per burst and a repetition rate of $1\,\mathrm{GHz}$.

In copper, the morphology at the optimal fluence is very different from the case of silicon. Fig. 7 compares as previously the single burst crater morphology at the optimal fluence for the different burst configurations. Remarkably, the craters present the same morphology independently from the repetition rate and the burst duration: they are mainly round (while the illumination is square) and show a smooth interior surface and a very thin wall all around that is typically only $60\,\mathrm{nm}$ thick. The walls tend to increase in height with the burst duration with a minimum of $1.4\,\mu\mathrm{m}$ for the shorter burst duration up to $2.8\,\mu\mathrm{m}$ for the longer burst. The difference can be due to the hotter material that needs more time to cool down, allowing the wall to grow more before resolidifying, or to a higher quantity of melted material that is pushed radially outward. As introduced previously, the presence of the thin rim has been recently

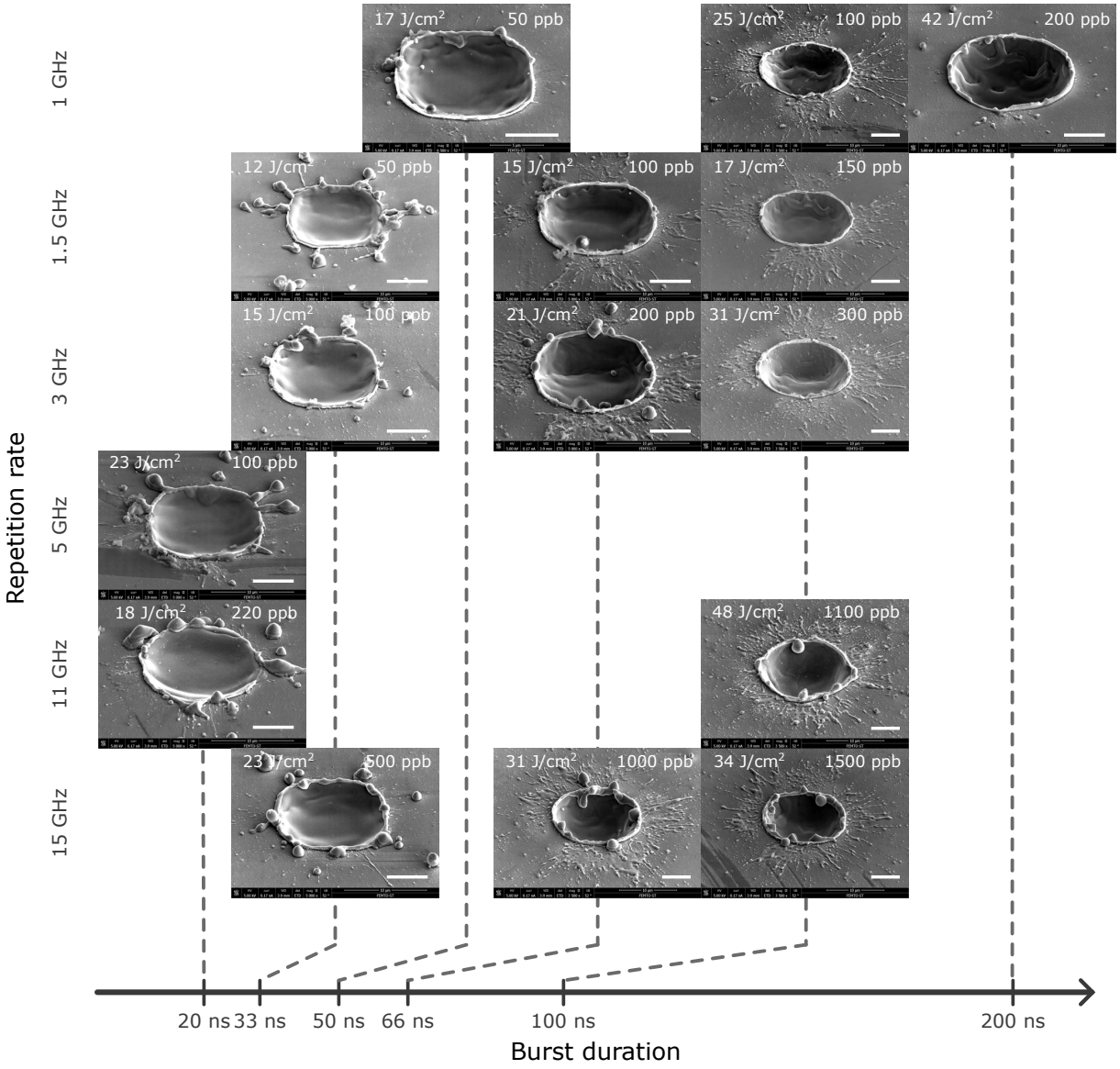


Figure 6: Comparison of the morphology of the craters in silicon at the optimal fluence of the tested configurations. The burst duration increases from left to right and the repetition rate from top to bottom. The optimal fluence and the number of sub-pulses per burst (ppb) are indicated in each sub-figure. Scale bars are $5\,\mu\mathrm{m}$.

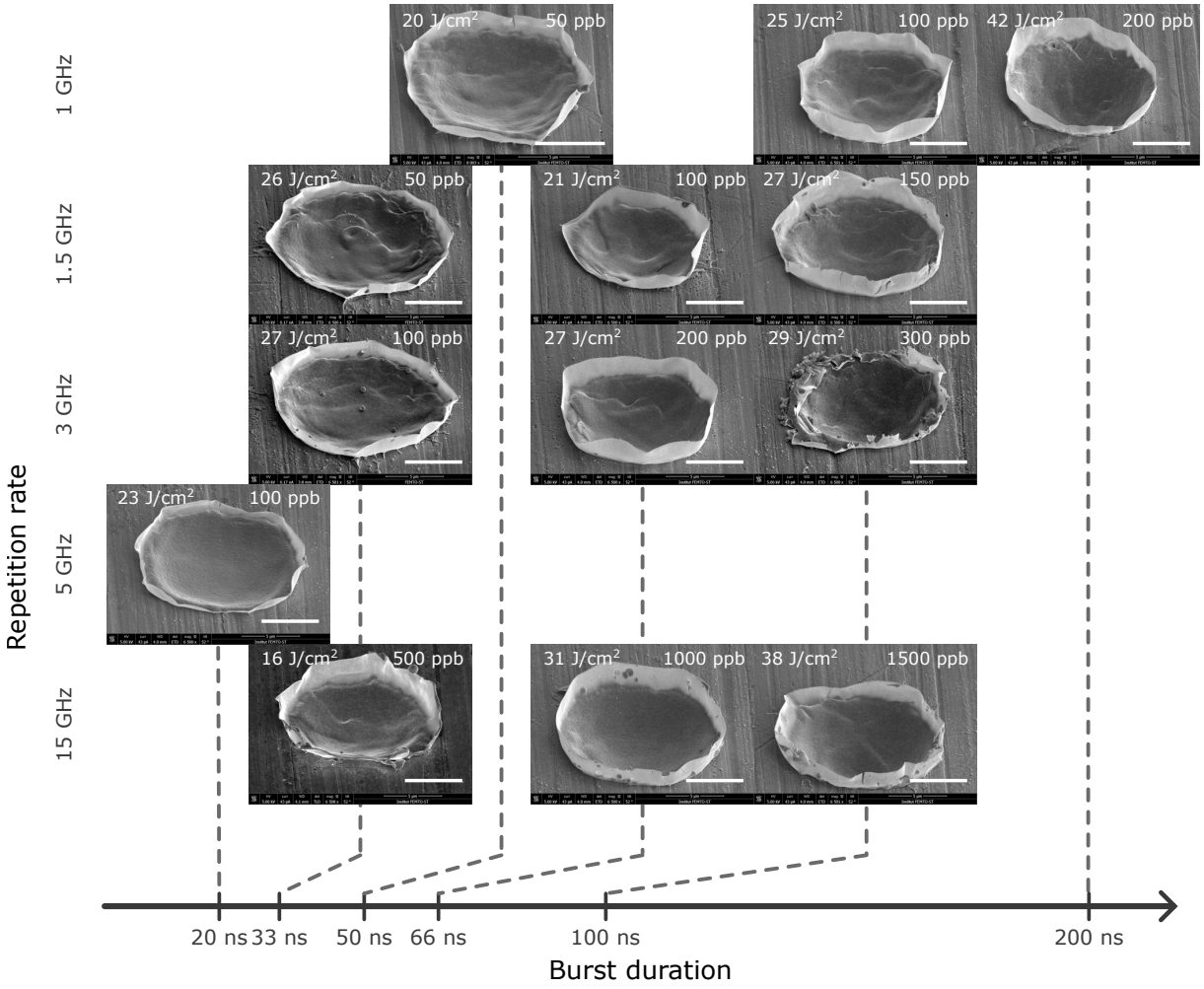


Figure 7: Comparison of the morphology of the craters in copper at the optimal fluence of the tested configurations. The burst duration increases from left to right and the repetition rate from top to bottom. The optimal fluence and the number of sub-pulses per burst (ppb) are indicated in each sub-figure. Scale bars are $5\,\mu\mathrm{m}$.

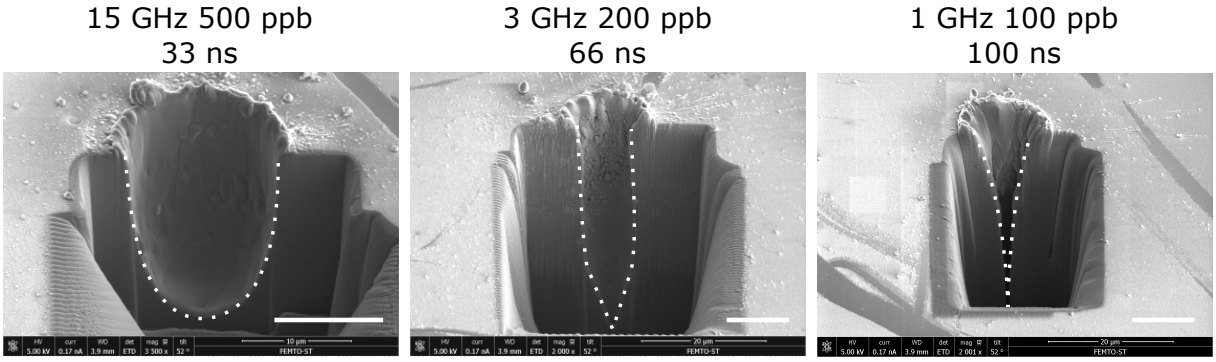


Figure 8: Cross-cut of the craters ablated in silicon with ten bursts for three different configurations at the burst fluence of $\approx 24\,\mathrm{J\,cm^{-2}}$ (close to the optimal fluence for the corresponding single burst case). Scale bars are $10\,\mu\mathrm{m}$. The white dotted lines highlight the crater profiles.

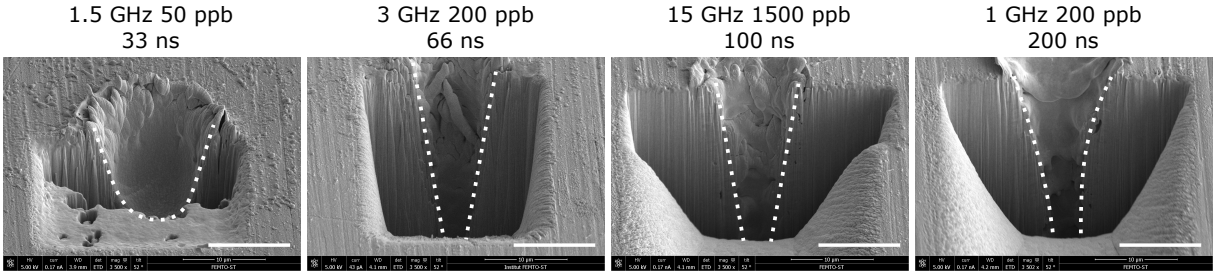


Figure 9: Cross-cut of the craters ablated in copper with ten bursts for four different configurations at the burst fluence of 50-60 $\mathrm{J\,cm^{-2}}$. Scale bars are $10\,\mu\mathrm{m}$. The white dotted lines highlight the crater profiles.

shown in literature for a Gaussian beam with 200 pulses per burst at $1.28\,\mathrm{GHz}$ and with sub-pulse fluence very close to our optima [11].

Noticeably, while the ablation by Gaussian beam in Ref. [11] led to craters surrounded also by small ejecta of molten material, here, we observe a very clean ablation with absence of ejecta around. We infer that the flat top profile may help to create a higher gradient of temperature in the molten material and, therefore, a cleaner ablation.

## 5 Percussion drilling

In the case of percussion drilling, the results are strikingly different between long and short bursts. We show in Fig. 8 for silicon and Fig. 9 for copper, SEM images of craters obtained for 10 bursts at an inter-burst repetition rate of $10\,\mathrm{kHz}$, at the optimal fluence. The burst duration increases from left to right. The white dotted lines highlight the crater profiles. At 33 ns burst duration, the craters are $13\,\mu\mathrm{m}$

| | 1.5 GHz - 50 ppb | 3 GHz - 100 ppb | 15 GHz - 500 ppb |
|---|---|---|---|
| Silicon | 0.63 ($11\,\mathrm{J\,cm^{-2}}$) | 0.71 ($15\,\mathrm{J\,cm^{-2}}$) | 0.67 ($23\,\mathrm{J\,cm^{-2}}$) |
| Copper | 0.16 ($50\,\mathrm{J\,cm^{-2}}$) | 0.19 ($50\,\mathrm{J\,cm^{-2}}$) | 0.21 ($47\,\mathrm{J\,cm^{-2}}$) |

Table 2: Optimal ablation efficiency in $\mathrm{mm^3/W/min}$ for copper and silicon for 10 bursts in percussion drilling. In parentheses, we indicate the corresponding burst fluence

wide (slightly larger than the beam FWHM) with vertical walls and nearly flat termination. In contrast, when the burst duration increases, the craters become deeper and highly tapered. Importantly, the same burst duration leads to a similar crater morphology independently from the other burst parameters.

We attribute the morphological change to the modification of the ablation plume evacuation dynamics. While longer burst durations induce an overall higher temperature of the melt phase as seen in previous section, we interpret that, in these burst conditions, less energy is transferred to the plume, *i.e.,* the vapor phase is less hot and with lower kinetic energy, which can explain the lower material removal, lower transmission of following laser pulses and subsequent morphology change in percussion drilling. This deforms the incoming beam and modifies the crater shape.

We then focused our characterization efforts on ablation efficiency of the best morphological case, *i.e.,* for the shortest burst duration of 33 ns. We report in Table 2 the *optimal* ablation efficiency values for three repetition rates together with the corresponding fluence.

We first notice that, in the case of silicon, the optimal fluence is the same as for single burst processing. It is interesting to compare the ablation efficiency obtained with a single burst and ten bursts. In silicon, the optimal ablation efficiency for the shortest burst duration is about $0.7\,\mathrm{mm^3/W/min}$ for the ten burst processing (as shown in Table 2) against the $0.4\,\mathrm{mm^3/W/min}$ of the single burst. The increase in the ablation efficiency can be explained by the incubation effect resulting from the multi-burst processes [27]. Importantly, in contrast with the tendency of the single burst processing, increasing the burst duration leads to a decrease of the ablation efficiency: $0.6\,\mathrm{mm^3/W/min}$ for the $66\,\mathrm{ns}$ burst and $0.3\,\mathrm{mm^3/W/min}$ for the $100\,\mathrm{ns}$ burst. The reduction of the ablation efficiency with the burst duration can be explained by the tapering of the hole and subsequent difficulties of the plasma plume to be evacuated from the crater.

We performed the same study on copper and present the results in Table 2. In this case, the optimal fluence of the multi-burst processing for the short burst duration differs from the single burst one: in general, the ten burst processing requires an optimal fluence that is twice the one of the single burst processing. The optimal ablation efficiency for the shortest burst duration is about twice lower than that of single-burst processing (with a maximum of $0.2\,\mathrm{mm^3/W/min}$). This contrasts with the results for silicon. We additionally note a starking difference: in silicon, particularly for short burst duration, the crater walls remain smooth and there is minimal resolidified material within the crater. In copper, however, resolidified material is clearly apparent along the crater edge and, with longer burst durations,

all along the crater wall. Since copper is more viscous than silicon, the removal of the melt material from the bottom of the crater may be more difficult for copper. The material pushed upward in the crater tends to resolidify on the walls, reducing the beam propagation and the process efficiency.

## 6 Conclusions

In this paper, we presented our results of single and multi-burst processing of silicon and copper samples, using burst durations ranging from $33\,\mathrm{ns}$ to $200\,\mathrm{ns}$. We explored a new range of burst repetition rates, ranging from $1\,\mathrm{GHz}$ up to $15\,\mathrm{GHz}$. While the ablation efficiency aligns with the values reported in the literature, we identified some previously unobserved trends.

We confirmed that longer burst durations increase the ablation efficiency. In terms of burst repetition rate, copper benefits from very high repetition rates, consistent with its higher thermal diffusivity, where silicon shows no advantages beyond a few GHz. It is therefore an advantage to be able to adapt the burst parameters to the material being processed. For silicon, the cleanest ablation is observed at lower repetition rates and longer bursts, while copper maintains a consistent morphology across all tested parameters. The crater morphologies suggest that a significant amount of molten material has been ejected from the crater. We observed similarities between the crater shapes and the splash patterns formed by a liquid reservoir due to a droplet impact. The different forms of ejection found around the craters in both materials find explanation with the material viscosities and the different maximum temperatures reached during the ablation process.

Lastly, we examined the crater evolution using ten bursts. In both materials, the craters tend to narrow as the burst duration increases. This is consistent with the difficulty of removing material from the crater bottom and the change of the beam shape along the propagation direction. While certain configurations in silicon result in higher ablation efficiency compared to single burst processing, copper shows a significant reduction in efficiency with the multi burst processing.

This study broadens the existing literature on GHz-range burst laser processing, providing new insights to further clarify the mechanisms underlying ablation in this regime. It also confirms that different materials require different optimal burst configurations (number of sub-pulses, intra-burst repetition rate) to achieve optimal ablation efficiency.

## Funding

This project has received funding from H2020 European Research Council (ERC) under grant agreement 682032-PULSAR, the European Union's Horizon 2020 research and innovation program under grant agreement No 825246 kW-flexiburst, the French Agence Nationale de la Recherche, projects DENSE (ANR-21-CE08-0005) and EQUIPEX+ SMARTLIGHT platform (ANR-21-ESRE-0040), and the EIPHI Graduate School (ANR-17-EURE-0002), and the Région Bourgogne Franche-Comté. This work was

partially supported by the French Renatech network and MIMENTO technological facility.

## Acknowledgment

The authors thank CAILABS for the Canunda-pulse module.

## Disclosures

The authors declare no conflicts of interest.

## Data availability

Data underlying the results presented in this paper are not publicly available at this time but may be obtained from the authors upon reasonable request.

1. Chichkov, B. N., Momma, C., Nolte, S., von Alvensleben, F. & Tünnermann, A. Femtosecond, picosecond and nanosecond laser ablation of solids. *Applied Physics A* **63**, 109–115 (1996).

2. Domke, M., Matylitsky, V. V. & Stroj, S. Surface ablation efficiency and quality of fs lasers in single-pulse mode, fs lasers in burst mode, and ns lasers. *Applied Surface Science* **505**, 144594 (2020).

3. Kerse, C. *et al.* Ablation-cooled material removal with ultrafast bursts of pulses. *Nature* **537** (2016).

4. Sugioka, K. Will ghz burst mode create a new path to femtosecond laser processing? *International Journal of Extreme Manufacturing* **3**, 043001 (2021). URL `https://dx.doi.org/10.1088/2631-7990/ac2479`.

5. Bonamis, G. *et al.* Systematic study of laser ablation with ghz bursts of femtosecond pulses. *Opt. Express* **28**, 27702–27714 (2020).

6. Hodgson, N., Allegre, H., Starodoumov, A. & Bettencourt, S. Femtosecond laser ablation in burst mode as a function of pulse fluence and intra-burst repetition rate. *Journal of Laser Micro/Nanoengineering* **15** (2020).

7. Matsumoto, H., Lin, Z., Schrauben, J. N. & Kleinert, J. Ultrafast laser ablation of silicon with GHz bursts. *Journal of Laser Applications* **33**, 032010 (2021). URL `https://doi.org/10.2351/7.0000372`.

8. Ye, H. *et al.* High-power nonlinear amplification of an ultrafast electro-optic frequency comb with flexible ghz repetition rate. *Optics Express* **30**, 10605–10613 (2022).

9. Hirsiger, T. *et al.* Machining metals and silicon with ghz bursts: Surprising tremendous reduction of the specific removal rate for surface texturing applications. In *Laser Applications in Microelectronic and Optoelectronic Manufacturing (LAMOM) XXV*, vol. 11267, 79–90 (SPIE, 2020).

10. Mishchik, K. *et al.* High-efficiency femtosecond ablation of silicon with ghz repetition rate laser source. *Opt. Lett.* **44**, 2193–2196 (2019).

11. Park, M., Gu, Y., Mao, X., Grigoropoulos, C. P. & Zorba, V. Mechanisms of ultrafast ghz burst fs laser ablation. *Science advances* **9**, eadf6397 (2023).

12. Okawa, T., Kubo, K., Kawai, K. & Kitabayashi, S. Experiments on splashing thresholds during single-drop impact onto a quiescent liquid film. *Experimental Thermal and Fluid Science* **121**, 110279 (2021).

13. Pavlov, D., Gurbatov, S., Kudryashov, S., Gurevich, E. & Kuchmizhak, A. Laser-induced surface relief nanocrowns as a manifestation of nanoscale rayleigh-plateau hydrodynamic instability. *Applied Surface Science* **511**, 145463 (2020).

14. Zhang, L. V., Brunet, P., Eggers, J. & Deegan, R. D. Wavelength selection in the crown splash. *Physics of Fluids* **22** (2010).

15. Assael, M. J. *et al.* Reference Data for the Density and Viscosity of Liquid Copper and Liquid Tin. *Journal of Physical and Chemical Reference Data* **39**, 033105 (2010). URL `https://doi.org/10.1063/1.3467496`.

16. Sato, Y. *et al.* Viscosity of molten silicon and the factors affecting measurement. *Journal of Crystal Growth* **249**, 404–415 (2003).

17. Neuenschwander, B. *et al.* processing of dielectric materials and metals with ps-laserpulses" 2010 icaleo conf. *Proc M* **101** (2010).

18. Hashida, M. *et al.* Ablation threshold dependence on pulse duration for copper. *Applied Surface Science* **197-198**, 862–867 (2002). URL `https://www.sciencedirect.com/science/article/pii/S0169433202004634`.

19. Jeschke, H. O. *et al.* Laser ablation thresholds of silicon for different pulse durations: theory and experiment. *Applied Surface Science* **197-198**, 839–844 (2002). URL `https://www.sciencedirect.com/science/article/pii/S0169433202004580`.

20. Bristow, A. D., Rotenberg, N. & van Driel, H. M. Two-photon absorption and kerr coefficients of silicon for 850–2200nm. *Applied Physics Letters* **90**, 191104 (2007).

21. Yilbas, B. S., Danisman, K. & Yilbas, Z. Measurement of temperature-dependent reflectivity of cu and al in the range 30-1000 degrees c. *Measurement Science and technology* **2**, 668 (1991).

22. Williams, E. & Brousseau, E. Nanosecond laser processing of zr41.2ti13.8cu12.5ni10be22.5 with single pulses. *Journal of Materials Processing Technology* **232**, 34–42 (2016). URL `https://www.sciencedirect.com/science/article/pii/S0924013616300231`.

23. Pure copper - thermal diffusivity. URL https://analyzing-testing.netzsch.com/en/applications/metals-alloys/pure-copper-thermal-diffusivity. Last accessed: 29 October 2024.

24. Parviz Elahi and Onder Akcaalan and Cansu Ertek and Koray Eken and F. Omer Ilday and Hamit Kalaycoglu. High-power Yb-based all-fiber laser delivering 300 fs pulses for high-speed ablation-cooled material removal. *Opt. Lett.* **43**, 535–538 (2018).

25. Matsumoto, H., Lin, Z. & Kleinert, J. Ultrafast laser ablation of copper with GHz bursts. In Neuenschwander, B., Grigoropoulos, C. P., Makimura, T. & Račiukaitis, G. (eds.) *Laser Applications in Microelectronic and Optoelectronic Manufacturing (LAMOM) XXIII*, vol. 10519, 1051902. International Society for Optics and Photonics (SPIE, 2018).

26. Bonamis, G. *et al.* High efficiency femtosecond laser ablation with gigahertz level bursts. *Journal of Laser Applications* **31**, 022205 (2019).

27. Zhang, R., McDowell, A., Hegmann, F., Fedosejevs, R. & Tsui, Y. Y. A study of incubation effects in femtosecond laser irradiation of silicon and copper. *Applied Physics A* **129**, 131 (2023).